01 Oct 2022

Triple-Differential Cross Sections in Three-Dimensional Kinematics for Electron-Impact-Ionization Dynamics of Tetrahydrofuran at 250-Ev Projectile Energy

Xiaorui Xue

Deepthy Maria Mootheril

Esam Ali

Maomao Gong

et. al. For a complete list of authors, see https://scholarsmine.mst.edu/phys_facwork/2230

Recommended Citation

X. Xue and D. M. Mootheril and E. Ali and M. Gong and S. Jia and J. Zhou and E. Wang and J. X. Li and X. Chen and D. H. Madison and A. Dorn and X. Ren, "Triple-Differential Cross Sections in Three-Dimensional Kinematics for Electron-Impact-Ionization Dynamics of Tetrahydrofuran at 250-Ev Projectile Energy," *Physical Review A*, vol. 106, no. 4, article no. 042803, American Physical Society, Oct 2022.
The definitive version is available at https://doi.org/10.1103/PhysRevA.106.042803

Triple-differential cross sections in three-dimensional kinematics for electron-impact-ionization dynamics of tetrahydrofuran at 250-eV projectile energy

Xiaorui Xue,[1] Deepthy Maria Mootheril,[2] Esam Ali,[3,4] Maomao Gong,[5,6] Shaokui Jia,[1] Jiaqi Zhou,[1,2] Enliang Wang,[5,6,2] Jian-Xing Li,[1] Xiangjun Chen,[5,6] Don Madison,[7,*] Alexander Dorn,[2] and Xueguang Ren[1,2,†]

[1]*School of Physics, Xi'an Jiaotong University, Xi'an 710049, China*

[2]*Max-Planck-Institut für Kernphysik, 69117 Heidelberg, Germany*

[3]*Department of Natural Sciences, D. L. Hubbard Center for Innovation, Northwest Missouri State University, Maryville, Missouri 64468, USA*

[4]*Department of Physics, Faculty of Arts and Sciences-El Marj, University of Benghazi, El Marj 9480, Libya*

[5]*Hefei National Laboratory for Physical Sciences at Microscale and Department of Modern Physics, University of Science and Technology of China, Hefei, Anhui 230026, China*

[6]*Synergetic Innovation Center of Quantum Information and Quantum Physics, University of Science and Technology of China, Hefei, Anhui 230026, China*

[7]*Department of Physics, Missouri University of Science and Technology, Rolla, Missouri 65409, USA*

(Received 25 July 2022; accepted 20 September 2022; published 7 October 2022)

We report a combined experimental and theoretical study of the ionization dynamics of tetrahydrofuran induced by 250 eV electron impact in which the highest occupied molecular orbital is ionized leading to the stable parent ion. Experimentally a reaction microscope was used, covering nearly the entire 4π solid angle for the ejected slow electron. We present the triple-differential cross sections for the projectile scattering angles of $\theta_1 = -10^\circ$ as a function of the emission angle of the ejected electrons with energies of $E_2 = 10$, 15, and 20 eV, i.e., for asymmetric energy sharing between the scattered and ejected electrons. The measured triple-differential cross sections are internormalized across the three ejected energies. The experimental data are compared with predictions from the molecular three-body distorted-wave (M3DW), the multicenter distorted-wave (MCDW) approaches, and a modified MCDW-WM method which includes the postcollision interaction using the Ward-Macek approximation. Generally, the M3DW cross sections show better agreement with experiment than the MCDW calculations except for the emission angles near the projectile forward direction. The MCDW and MCDW-WM calculations do not reproduce the recoil lobes and show very small intensity for the cross sections outside the scattering plane.

DOI: 10.1103/PhysRevA.106.042803

I. INTRODUCTION

Electron-impact-ionization cross sections are relevant in many fields of science and technical applications. For example, the study of the ionizing collisions between incident electrons and atoms or molecules enabled scientists for many years to explore the few-body quantum dynamics, and to obtain electronic structure information of gaseous or condensed matter [1–3]. On the other hand, these studies can give relevant data for modeling collision processes, not only in natural environments such as the upper atmosphere and interstellar space, but also in technical plasmas, nuclear reactors, and in medical radiation therapy [4–7]. It has been well established that lesions, e.g., in DNA, are not only caused by the high-energy primary radiation, but also by the abundant secondary electrons which have been found to effectively induce strand breaks in DNA and the subunits [7–10]. Providing cross sections of processes involving the interactions of electrons with biomolecules is essential for understanding the biological damage induced by ionizing radiation.

Complete information on the ionization dynamics can be obtained by kinematically complete experiments, or so-called $(e, 2e)$ studies, in which the linear momentum vectors of all final-state particles are determined [1,2]. The quantity measured in such experiments is the triple-differential cross sections (TDCSs), which serves as a powerful tool to test theoretical models that account for the quantum-mechanical few-body interactions. Experimental techniques like reaction microscope allow one to access a large fraction of the entire solid angle and a range of energies of the continuum electrons in the final state [11–13], and for the measurement of absolute cross sections [14]. Thus, theories can be tested more comprehensively over a large range of the final-state phase space.

For simple atoms and molecules, the measured TDCSs can be well reproduced by the most sophisticated nonperturbative theories [15–22]. On the other hand, advanced perturbative

*Deceased.

†renxueguang@xjtu.edu.cn

models are more tractable, and can be applied to larger systems including biomolecules (see, e.g., [23–35]). Additionally, they give information about which interactions are relevant and which reaction mechanisms occur. TDCSs are now also being considered as input parameters for Monte Carlo simulations of track structures of energetic ionizing particles or radiation to predict the damage done to living tissues. Consequently, there have been recent systematic investigations of the ionization dynamics of biomolecules, e.g., for tetrahydrofuran (THF, C_4H_8O), which can be regarded as a molecular analog of the deoxyribose sugar ring in the DNA backbone [30–35]. Experimentally, studies of THF have been performed in the coplanar asymmetric geometry at $E_0 = 250$ eV using a conventional $(e, 2e)$ spectrometer [34,35]. A number of theoretical models were developed to compare with the experimental TDCSs [30–33], where the different theories show larger discrepancies with experiment and also between each other, particularly for the recoil pattern and the relative magnitude between binary and recoil lobes [33]. It is difficult to reflect on the quality of the theoretical models since the experiments do not show a sufficient good statistical significance.

In the present work, we perform a kinematically complete experiment of electron-impact ionization of THF at 250 eV projectile energy using a reaction microscope [11–13], in which the three-dimensional (3D) momentum vectors of two outgoing electrons and the recoil ion were measured in triple coincidence. Here, ionization of $9b$ and $12a'$ orbitals, corresponding to the highest occupied molecular orbital (HOMO) of C_2 and C_s conformers of THF, respectively, are observed, which lead to an intact $C_4H_8O^+$ ion in the final state [36]. The TDCSs were measured by covering a large part of the full solid angle for the emitted electron. The measurements reported here cover a range of ejected electron energies ($E_2 =$ 10, 15, and 20 eV) with a projectile scattering angle of $\theta_1 = -10^\circ$. The obtained TDCSs are internormalized for different ejection energies, which means that a single scaling factor is sufficient to put the experimental cross sections on an absolute scale. The experimental data are compared with theoretical predictions from both the multicenter distorted-wave [31] and the molecular three-body distorted-wave approaches [33].

II. EXPERIMENTAL METHOD

Experiments were carried out using a multiparticle momentum imaging spectrometer (reaction microscope) combined with a photoemission electron source and a heatable gas jet. This technique was described in detail elsewhere (see, e.g., [11–13]), so only a brief outline will be given here. The well-collimated electron beam with the energy of $E_0 = 250$ eV is crossed with a supersonic gas jet. Different from the previous gas targets (argon, neon, etc.), the sample in this experiment is liquid, with a vapor pressure sufficient to generate a seeded expansion of He gas (1 bar) [37].

The pulsed electron beam ($\Delta T \approx 0.5$ ns and $\Delta E_0 \approx 0.5$ eV) is produced by a pulsed ultraviolet laser beam ($\lambda =$ 266 nm) irradiating a tantalum photocathode [36]. After collision the fragment ion and electron are extracted by homogeneous magnetic and electric fields toward two position- and time-sensitive microchannel plate detectors equipped with fast multihit delay-line anodes. The unscattered primary beam is dumped to the central bore in the electron detector without inducing a signal. For single ionization of THF, we use the triple-coincidence detection of two outgoing electrons and one recoil ion constituting a kinematically complete measurement. The 3D vectors of the final-state electrons and ions are determined from the measured times-of-flight and positions. The detection solid angle for the $C_4H_8O^+$ ion is 4π. The acceptance angle for detection of electrons up to an energy of 20 eV is also close to 4π, except for the acceptance holes at small forward and backward angles where the electrons end up in the detector bore. The momentum vectors of two outgoing electrons were measured directly without relying on the recoil-ion momentum. This allows for $(e, 2e)$ studies on heavy and warm targets with the reaction microscope.

For the present focus diameter of 1 mm and the pulse width of 0.5 ns the momentum resolution of electrons is better than 0.1 a.u. [38]. As a result, for the angular resolution the following upper limits are obtained (full width at half maximum): $\Delta\phi = 6^\circ$ for the azimuth angles of both the fast and slow final-state electrons and $\Delta\theta_1 = 2^\circ$ and $\Delta\theta_2 = 6^\circ$ for the polar angles of the fast and slow electrons, respectively. The coincidence binding energy ($E_b = E_0 - E_1 - E_2$) resolution is determined to be $\Delta E_b \sim 8.0$ eV, which is not sufficient to uniquely identify the ionized molecular orbital. On the other hand, the coincident detection of the residual ion provides a restriction on the contributing orbitals. Here, the intact $C_4H_8O^+$ ions are solely attributable to the HOMO ionization of THF [36].

III. THEORETICAL MODELS

In the theoretical calculations, we used three different methods to describe the present electron-impact-ionization process, namely, the molecular three-body distorted-wave approach (M3DW), the multicenter distorted-wave (MCDW) approximation, and a modified MCDW-WM method. Details about the calculations have been discussed previously in Refs. [23,33] for M3DW and Refs. [28,31] for the calculations based on MCDW. The M3DW model contains the final-state Coulomb-distortion factor between the two electrons, normally called the postcollision interaction (PCI) exactly. In the MCDW method, the incident and scattered electrons are described by plane waves and the ejected electron is described by a multicenter distorted wave calculated using an anisotropic distortion potential. The MCDW retains the nuclear term in the Bethe integral and does not include PCI. We have also introduced the PCI effect into the MCDW-WM calculation by the so-called Gamow factor using the Ward-Macek approximation [39]. More information can be found in the references given.

IV. RESULTS AND DISCUSSIONS

The THF molecule has two conformers; their relative populations are dependent on the temperature [40]. The C_2 conformer is the dominant one close to zero temperature and its population decreases with increasing temperature. In this experiment, the average temperature of the target is estimated to be roughly 30 K, which corresponds to a branching ratio of

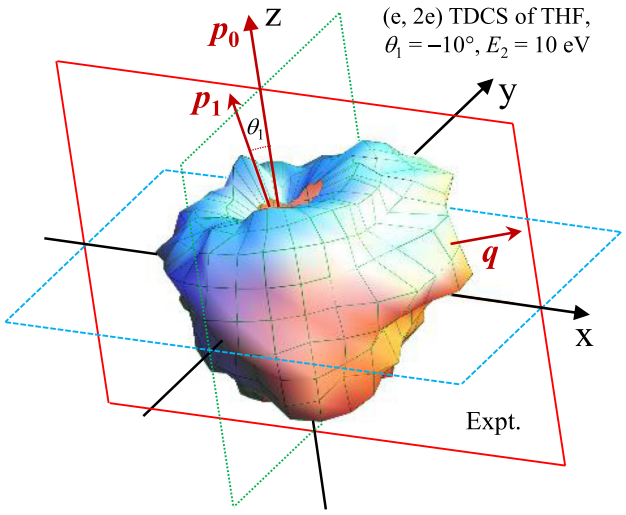

FIG. 1. Experimental TDCS in three-dimensional representation for the HOMO ionization of THF ($0.8 \times 9b + 0.2 \times 12a'$) by incident electrons with energy of $E_0 = 250$ eV. The scattering angle is $\theta_1 = -10°$, and the ejected electron energy is $E_2 = 10$ eV.

about 80% : 20% for the C_2 to C_s conformer [40]. Moreover, the coincident detection of the residual ion provides a restriction on the number of contributing orbitals. Here only the production of intact $C_4H_8O^+$ cations is considered. Therefore, the experimental data represent the summed TDCS for the HOMO ionization of the two conformers [36], i.e., ionization of $9b$ (80%) and $12a'$ (20%).

Figure 1 presents the experimental TDCS as a 3D polar plot for a projectile scattering angle of $\theta_1 = -10°$ as a function of the emission direction of a slow ejected electron with $E_2 = 10$ eV energy. In this 3D image, the TDCS for a particular direction is given as the distance from the origin of the plot to the point on the surface, which is intersected by the emission direction of the ejected electron. The projectile (p_0) enters from the bottom and is scattered to the left with a momentum vector p_1. The plane where the vectors p_0 and p_1 are located is defined as the scattering ($x - z$) plane as indicated by the solid frame in Fig. 1. The momentum transfer to the target is indicated by the arrow labeled q, which is determined as $p_0 - p_1$. In the discussion below, the two electrons generated in the ($e, 2e$) process are defined as follows: the slower one is called the ejected electron, and the faster one is called the scattered electron.

In the 3D TDCS, the emission pattern of the ejected electrons can be roughly classified into two main features. The binary lobe is oriented along the momentum transfer q corresponding to electrons emitted in a single binary collision between the projectile and target electron. In the opposite direction the recoil lobe is formed, where the ejected electron additionally backscatters in the molecular potential. Compared to the 3D TDCS for argon atoms at a similar impact energy [38], the present result depicts a significant change of the shape and the relative size of both binary and recoil lobes. The two lobes tend to merge or are partially superimposed on one another and thus fill the minimum separating the binary from the recoil lobe, leading to a somehow isotropic distribution. This might result from the multicenter nature of the residual $C_4H_8O^+$ ion potential. Furthermore, the ejected electron is repelled by the scattered projectile due to the long-range nature of the Coulomb force. This PCI effect can rotate the binary peak to larger scattering angles relative to the momentum transfer q direction. At the present intermediate- to high-energy regime, the influence of PCI can be comparatively smaller than in the case of low-impact energy collisions [14,40].

For a quantitative study of TDCS over a large range of the measured phase space, we present cuts through the 3D TDCS for the three orthogonal planes of the ejected electron as indicated in Fig. 1 by the solid, dashed, and dotted frames. In addition to the $x - z$ scattering plane mentioned above, the perpendicular plane (dotted frame) and the full-perpendicular plane (dashed frame) are defined as follows: The perpendicular $y - z$ plane contains the incoming beam axis and is perpendicular to the scattering plane. The full-perpendicular $x - y$ plane is perpendicular to the incoming projectile beam direction. The results discussed below are for a projectile scattering angle of $\theta_1 = -10°$, and for the ejected electron energies of $E_2 = 10$, 15, and 20 eV.

The experimental TDCSs are presented in Figs. 2–4 as a function of the ejected-electron emission angles, and are compared with calculations from the M3DW and MCDW methods in the scattering, perpendicular, and full-perpendicular planes, respectively. The experimental cross sections are not absolute. The scaling factor used to normalize the experimental data to the theories was found by achieving a good visual fit of experiment and the calculations for the TDCS in the scattering plane at $\theta_1 = -10°$ and $E_2 = 20$ eV [Fig. 2(c)]. This factor was subsequently applied to all other kinematics and planes, i.e., the experimental data are consistently cross normalized to each other. The MCDW theoretical results are multiplied by a factor of 0.5 in order to compare with the results from experiment and other calculations.

Figure 2 shows the TDCSs in the scattering plane, which cuts through the binary and the recoil lobes and contains the momentum transfer vector q indicated in the diagrams by arrows. In this plane, the well-known binary and recoil patterns are more clearly revealed at the higher ejected energy of $E_2 = 20$ eV [Fig. 2(c)], whereas for the lower ejection energy of $E_2 = 10$ eV these two patterns tend to overlap, making it difficult to distinguish between them [Fig. 2(a)]. In addition, the binary lobe often exhibits a minimum or dip around the q direction. This is the result of the characteristic momentum profile of p-like orbitals; in particular, the $9b$ orbital of the C_2 conformer has a node for vanishing momentum [3].

Comparing the experimental data to the two sets of theoretical results, we see that the M3DW predictions are generally in good agreement with the experimental results, particularly regarding the angular dependence in the recoil region and the relative magnitude between binary and recoil lobes. In the binary region, the M3DW predicts a minimum near the q direction, which is much deeper than the experiment. The minimum position is slightly shifted to larger angles with respect to the q direction possibly due to the PCI effect, which is accounted for by M3DW. There are noticeable systematic discrepancies between M3DW and experiment observed for

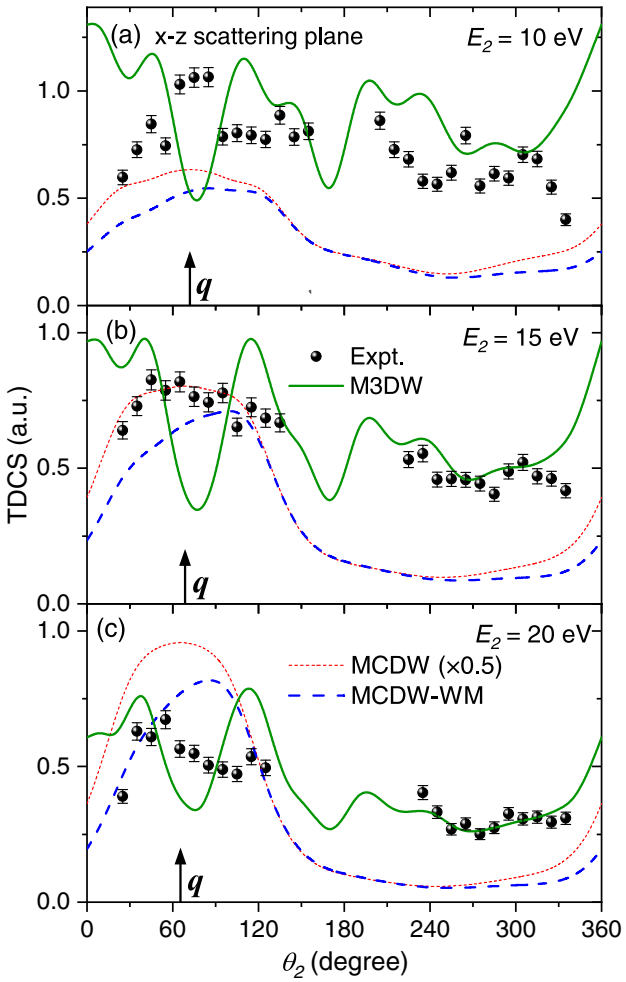

FIG. 2. Experimental and theoretical TDCSs in the $x-z$ scattering plane for the ionization of THF ($0.8 \times 9b + 0.2 \times 12a'$) as a function of the ejected electron's emission angle for a scattering angle of $\theta_1 = -10°$. (a)–(c) show the TDCSs for the ejected electron energies of $E_2 = 10$, 15, and 20 eV (from top to bottom panels). The solid circles with error bars represent the experimental data. Green solid lines: M3DW; red dotted lines: MCDW; blue dashed lines: MCDW-WM.

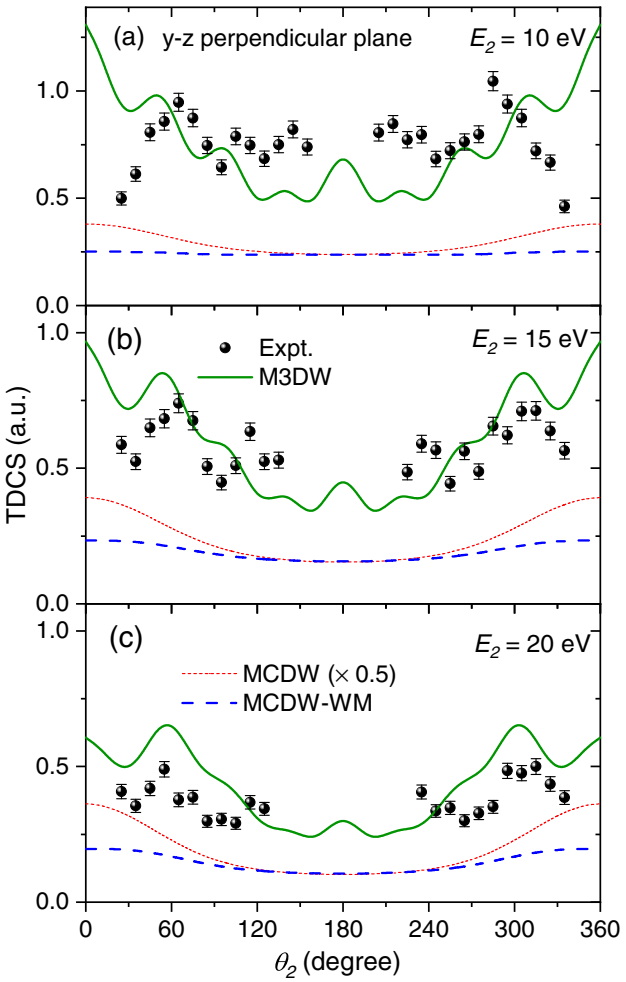

FIG. 3. Same as Fig. 2 but for the perpendicular plane.

emission angles near 0° and 360°, where the M3DW predicts a maximum while the experimental data show a minimum. On the other hand, the MCDW and MCDW-WM calculations show a reasonable agreement with the shape of the binary lobe, in particular for the ejection energy of $E_2 = 15$ eV in Fig. 2(b). Here, the MCDW-WM predicted cross sections for emission angles near 0° and 360° is lower than MCDW calculations due to the effect of PCI, which is accounted for in MCDW-WM via the Ward-Macek approximation [39]. The differences from the M3DW and the experiment are that the binary peak produced by these two calculations shows only a single peak for the energy conditions analyzed and the predicted magnitudes are higher for $E_2 = 20$ eV and lower for $E_2 = 10$ eV than in the experiment. Additionally, we have found that the MCDW and MCDW-WM calculations predict either no recoil peak or a much smaller one, which is not consistent with the experimental results.

Figure 3 shows a comparison between experiment and theory for the $y-z$ perpendicular plane. For this plane, symmetry considerations require the cross sections to be symmetric about 180°, which can indeed be seen in both theory and experiment. This plane cuts through the binary lobe which results in two symmetric maxima at θ_2 near 60° and 300° due to the high-order projectile-target interactions [38]. In addition, there is an indication of a rather flatter distribution of the cross sections in the angular range from 90° to 270°, which is particularly visible for the case of $E_2 = 10$ eV. Here, the M3DW is in much better agreement with experiment than the MCDW, where the magnitude and the angular dependance of the cross sections are rather well reproduced by the M3DW, especially when considering the two symmetric maxima. We note that the M3DW predicts some small peaks in the central region, which are also indicated in the experimental results in particular for the ejection energies of $E_2 = 10$ and 15 eV shown in Figs. 3(a) and 3(b), respectively. The M3DW also reveals a peak at θ_2 close to 180°; however, the cross section in this region is not accessible in the experiment. According to Ali *et al.* [33], these small peaks are a result of interference effects contained in the theoretical approach. Problems for the M3DW remain at θ_2 near the projectile forward direction (around 0° and 360°), where the predicted strong maxima are

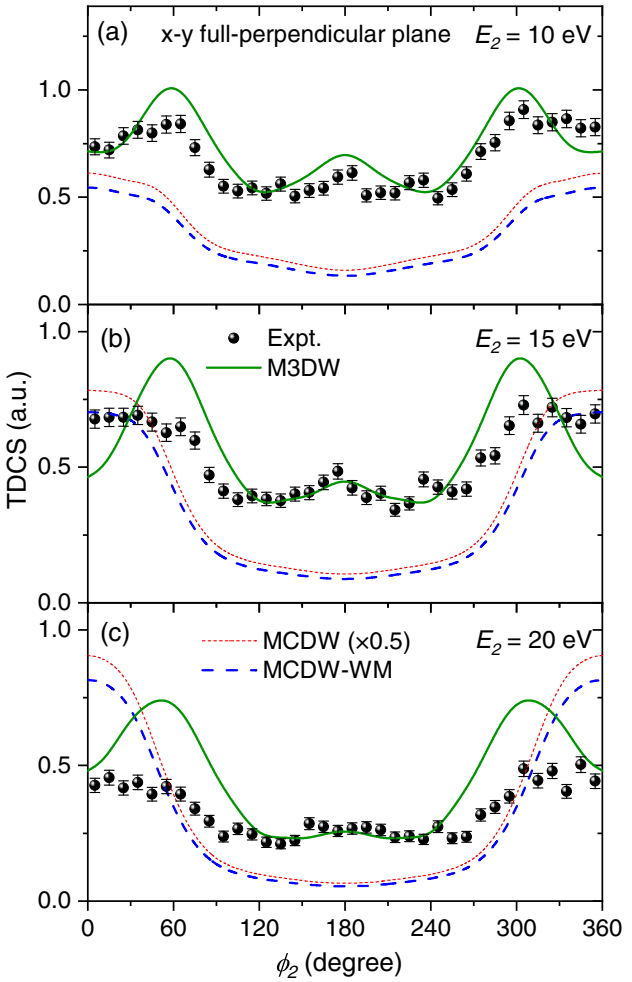

FIG. 4. Same as Fig. 2 but for the full-perpendicular plane.

not indicated by the experiment. This finding is similar to that noted above also for the scattering plane. The MCDW and MCDW-WM binary and recoil peaks are not contributing significantly to the y-z plane cross section and, consequently, all panels show that the predicted cross section is significantly smaller than observed experimentally. In this plane PCI can play a role for emission angles near 0° and 360° and, thus, the MCDW-WM predicted cross sections are lower than MCDW in the forward direction.

Figure 4 shows the comparison between experiment and theory for the full-perpendicular plane (i.e., the $x-y$ plane). Here, the polar angle (θ_2) of the ejected electron is fixed to 90° and the azimuthal angle ϕ_2 is varied. The experimental angular acceptance covers the entire 0°–360° range, but the cross sections are again symmetric with respect to 180°. The binary and recoil peaks are observed in the vicinity of $\phi_2 = 0°$ and 180°, respectively. The binary pattern contains two maxima at ϕ_2 near 60° and 300° for the ejection energy of $E_2 = 10$ eV, which becomes a broad maximum centered at ϕ_2 close to 0° and 360° for the cases of $E_2 = 15$ and 20 eV. For the recoil pattern, the cross sections show a maximum located at $\phi_2 = 180°$. These features are well reproduced by the M3DW calculations, in particular for the recoil peak and the two symmetric maxima for the binary lobe. The MCDW and MCDW-WM calculations show a broad peak for the emission angles close to 0° and 360°, which is in reasonable agreement with the shape of the binary lobes observed in Figs. 4(b) and 4(c) for the ejection energies of $E_2 = 15$ and 20 eV, respectively. However, these two calculations do not reproduce the recoil peak and show much smaller intensity in comparison with the experimental and M3DW results. In addition, it is seen that the cross sections predicted by the MCDW and MCDW-WM calculations are almost identical in this plane, which means that the influence of PCI appears to be small over the entire angular range.

V. CONCLUSION

In summary, we have reported a comprehensive study of the electron-impact-ionization dynamics of THF for a projectile energy of 250 eV and a scattering angle of $\theta_1 = -10°$. Experimentally, the three-dimensional momentum vectors of the final-state particles are determined for a large part of the solid angle for the slow emitted electron. Thus, full three-dimensional representations of the cross sections are accessible. The measured triple-differential cross sections for ionization of the HOMO of THF were internormalized across three ejected electron energies E_2 from 10 to 20 eV, thus providing a rigorous test bed for the theoretical models.

The experimental data are compared with results from the M3DW, MCDW, and MCDW-WM models. There is overall better agreement between the M3DW predictions and the experimental data than the MCDW calculations concerning both the angular dependence of the cross sections and the relative magnitude over the entire range of angle and energy conditions analyzed. Noticeable systematic discrepancies occur in the scattering and perpendicular planes (Figs. 3 and 4), where the M3DW predicted cross sections are significantly higher than that observed experimentally for the emission angles near the projectile forward direction. The MCDW and MCDW-WM calculations predict reasonably the shape of the binary lobes in the scattering and full-perpendicular planes; however, these two calculations show either no recoil peak or a very small one, which is not consistent with both experiment and M3DW results. Furthermore, in the perpendicular plane the cross sections from MCDW and MCDW-WM predictions show much smaller intensity and do not reproduce the structures observed experimentally. The fact that the two calculations using MCDW and M3DW models differ strongly with each other indicates that the theoretical treatment of the electron-impact ionization of larger biomolecules is very complex and the results are very sensitive to the details of the model employed. The present experimental data substantially enhance the still very limited set of data currently available to thoroughly test theoretical methods for more accurately describing the electron track structures in biorelevant systems [41,42].

ACKNOWLEDGMENTS

This work was jointly supported by the National Natural Science Foundation of China (NSFC) under Grants No. 11974272, No. 11774281, and No. 12004370; the Strategic

Priority Research Program of Chinese Academy of Sciences, Grant No. XDB34020000; the United States National Science Foundation under Grant No. OAC-1919789; and by the Deutsche Forschungsgemeinschaft (DFG). X.R. is grateful for support from the Open Fund of the State Key Laboratory of High Field Laser Physics (Shanghai Institute of Optics and Fine Mechanics.). J.Z. is grateful for support from the China Scholarship Council (CSC).

[1] H. Ehrhardt, K. Jung, G. Knoth, and P. Schlemmer, Differential cross sections of direct single electron impact ionization, Z. Phys. D **1**, 3 (1986).

[2] A. Lahmam-Bennani, Recent developments and new trends in *(e,2e) and (e,3e)* studies, J. Phys. B: At., Mol. Opt. Phys. **24**, 2401 (1991).

[3] I. E. McCarthy and E. Weigold, Electron momentum spectroscopy of atoms and molecules, Rep. Prog. Phys. **54**, 789 (1991).

[4] K. Bartschat and M. J. Kushner, Electron collisions with atoms, ions, molecules, and surfaces: Fundamental science empowering advances in technology, Proc. Natl. Acad. Sci. USA **113**, 7026 (2016).

[5] L. Campbell and M. J. Brunger, Electron collisions in atmospheres, Int. Rev. Phys. Chem. **35**, 297 (2016).

[6] B. C. Garrett, D. A. Dixon, D. M. Camaioni, D. M. Chipman, M. A. Johnson, C. D. Jonah, G. A. Kimmel, J. H. Miller, T. N. Rescigno, P. J. Rossky *et al.*, Role of water in electron-initiated processes and radical chemistry: Issues and scientific advances, Chem. Rev. **105**, 355 (2005).

[7] E. Alizadeh, T. M. Orlando, and L. Sanche, Biomolecular damage induced by ionizing radiation: The direct and indirect effects of low-energy electrons on DNA, Annu. Rev. Phys. Chem. **66**, 379 (2015).

[8] S. M. Pimblott and J. A. LaVerne, Production of low-energy electrons by ionizing radiation, Radiat. Phys. Chem. **76**, 1244 (2007).

[9] M. A. Huels, B. Boudaïffa, P. Cloutier, D. Hunting, and L. Sanche, Single, double, and multiple double strand breaks induced in DNA by 3–100 eV electrons, J. Am. Chem. Soc. **125**, 4467 (2003).

[10] J. Zhou, X. Yu, S. Luo, X. Xue, S. Jia, X. Zhang, Y. Zhao, X. Hao, L. He, C. Wang, D. Ding, and X. Ren, Triple ionization and fragmentation of benzene trimers following ultrafast intermolecular Coulombic decay, Nat. Commun. **13**, 5335 (2022).

[11] J. Ullrich, R. Moshammer, A. Dorn, R. Dörner, L. P. H. Schmidt, and H. Schmidt-Böcking, Recoil-ion and electron momentum spectroscopy: Reaction-microscopes, Rep. Prog. Phys. **66**, 1463 (2003).

[12] M. Dürr, C. Dimopoulou, A. Dorn, B. Najjari, I. Bray, D. V. Fursa, Z. Chen, D. H. Madison, K. Bartschat, and J. Ullrich, Single ionization of helium by 102 eV electron impact: three-dimensional images for electron emission, J. Phys. B: At., Mol. Opt. Phys. **39**, 4097 (2006).

[13] X. Ren, S. Amami, K. Hossen, E. Ali, C. G. Ning, J. Colgan, D. Madison, and A. Dorn, Electron-impact ionization of H_2O at low projectile energy: Internormalized triple-differential cross sections in three-dimensional kinematics, Phys. Rev. A **95**, 022701 (2017).

[14] J. Zhou, E. Ali, M. Gong, S. Jia, Y. Li, Y. Wang, Z. Zhang, X. Xue, D. V. Fursa, I. Bray *et al.*, Absolute triple differential cross sections for low-energy electron impact ionization of biochemically relevant systems: Water, tetrahydrofuran, and hydrated tetrahydrofuran, Phys. Rev. A **104**, 012817 (2021).

[15] I. Bray, D. V. Fursa, A. S. Kadyrov, A. T. Stelbovics, A. S. Kheifets, and A. M. Mukhamedzhanov, Electron- and photon-impact atomic ionisation, Phys. Rep. **520**, 135 (2012).

[16] T. N. Rescigno, M. Baertschy, W. A. Isaacs, and C. W. McCurdy, Collisional breakup in a quantum system of three charged particles, Science **286**, 2474 (1999).

[17] J. Colgan, M. S. Pindzola, F. J. Robicheaux, D. C. Griffin, and M. Baertschy, Time-dependent close-coupling calculations of the triple-differential cross section for electron-impact ionization of hydrogen, Phys. Rev. A **65**, 042721 (2002).

[18] X. Ren, S. Amami, O. Zatsarinny, T. Pflüger, M. Weyland, W. Y. Baek, H. Rabus, K. Bartschat, D. Madison, and A. Dorn, Kinematically complete study of low-energy electron-impact ionization of neon: Internormalized cross sections in three-dimensional kinematics, Phys. Rev. A **91**, 032707 (2015).

[19] X. Ren, A. Senftleben, T. Pflüger, K. Bartschat, O. Zatsarinny, J. Berakdar, J. Colgan, M. S. Pindzola, I. Bray, D. V. Fursa, and A. Dorn, Propensity for distinguishing two free electrons with equal energies in electron-impact ionization of helium, Phys. Rev. A **92**, 052707 (2015).

[20] O. Zatsarinny and K. Bartschat, Nonperturbative Treatment of Ionization with Excitation of Helium by Electron Impact, Phys. Rev. Lett. **107**, 023203 (2011).

[21] X. Ren, T. Pflüger, S. Xu, J. Colgan, M. S. Pindzola, A. Senftleben, J. Ullrich, and A. Dorn, Strong Molecular Alignment Dependence of $\mathbf{H}_2$ Electron Impact Ionization Dynamics, Phys. Rev. Lett. **109**, 123202 (2012).

[22] X. Ren, K. Hossen, E. Wang, M. S. Pindzola, A. Dorn, and J. Colgan, Analysis of multiple scattering contributions in electron-impact ionization of molecular hydrogen, J. Phys. B: At., Mol. Opt. Phys. **50**, 204002 (2017).

[23] D. H. Madison and O. Al-Hagan, The distorted-wave born approach for calculating electron-impact ionization of molecules, J. At. Mol. Opt. Phys. **2010**, 367180 (2010).

[24] C. M. Granados-Castro and L. U. Ancarani, Electron impact ionization of the outer valence orbital $1t_2$ of CH_4, Eur. Phys. J. D **71**, 65 (2017).

[25] K. L. Nixon, A. J. Murray, O. Al-Hagan, D. H. Madison, and C. Ning, Low-energy symmetric coplanar and symmetric non-coplanar (e,2e) studies from the $3a_1$ state of H_2O, J. Phys. B: At., Mol. Opt. Phys. **43**, 035201 (2010).

[26] C.-Y. Lin, C. W. McCurdy, and T. N. Rescigno, Complex Kohn approach to molecular ionization by high-energy electrons: Application to H_2O, Phys. Rev. A **89**, 012703 (2014).

[27] E. Acebal and S. Otranto, Continuum-distorted-wave eikonal-initial-state description of the electron-impact ionization of H_2O at low impact energies, Phys. Rev. A **98**, 012703 (2018).

[28] S. Zhang, X. Y. Li, J. G. Wang, Y. Z. Qu, and X. Chen, Multicenter distorted-wave method for fast-electron-impact single ionization of molecules, Phys. Rev. A **89**, 052711 (2014).

[29] M. Gong, X. Li, S. B. Zhang, S. Niu, X. Ren, E. Wang, A. Dorn, and X. Chen, Multicenter three-distorted-wave approach to three-dimensional images for electron-impact-ionization dynamics of molecules: Overall agreement with experiment, Phys. Rev. A **98**, 042710 (2018).

[30] L. Mouawad, P.-A. Hervieux, C. D. Cappello, J. Pansanel, V. Robert, and Z. E. Bitar, Triple differential cross sections for the ionization of tetrahydrofuran by electron impact, J. Phys. B: At., Mol. Opt. Phys. **51**, 175201 (2018).

[31] X. Xu, M. Gong, X. Li, S. B. Zhang, and X. Chen, Theoretical study of (*e, 2e*) triple differential cross sections of tetrahydrofuran using multicenter distorted-wave method, J. Chem. Phys. **148**, 244104 (2018).

[32] P. Singh and C. Champion, Theoretical study of (*e, 2e*) triple-differential cross sections for DNA component ionization by electrons and positrons, J. Phys. B: At., Mol. Opt. Phys. **52**, 075201 (2019).

[33] E. Ali, H. S. Chakraborty, and D. H. Madison, Improved theoretical calculations for electron-impact ionization of DNA analogue molecules, J. Chem. Phys. **152**, 124303 (2020).

[34] C. J. Colyer, S. M. Bellm, B. Lohmann, G. F. Hanne, O. Al-Hagan, D. H. Madison, and C. G. Ning, Dynamical *(e, 2e)* studies using tetrahydrofuran as a DNA analog, J. Chem. Phys. **133**, 124302 (2010).

[35] D. Jones, J. Builth-Williams, S. Bellm, L. Chiari, H. Chaluvadi, D. Madison, C. Ning, B. Lohmann, O. Ingólfsson, and M. Brunger, Dynamical (*e,2e*) investigations of tetrahydrofuran and tetrahydrofurfuryl alcohol as DNA analogues, Chem. Phys. Lett. **572**, 32 (2013).

[36] X. Ren, T. Pflüger, M. Weyland, W. Y. Baek, H. Rabus, J. Ullrich, and A. Dorn, An (*e, 2e* + ion) study of low-energy electron-impact ionization and fragmentation of tetrahydrofuran with high mass and energy resolutions, J. Chem. Phys. **141**, 134314 (2014).

[37] X. Ren, E. Wang, A. D. Skitnevskaya, A. B. Trofimov, K. Gokhberg, and A. Dorn, Experimental evidence for ultrafast intermolecular relaxation processes in hydrated biomolecules, Nat. Phys. **14**, 1062 (2018).

[38] X. Ren, A. Senftleben, T. Pflüger, A. Dorn, K. Bartschat, and J. Ullrich, Signatures of projectile–nucleus scattering in three-dimensional (e,2e) cross sections for argon, J. Phys. B: At., Mol. Opt. Phys. **43**, 035202 (2010).

[39] S. J. Ward and J. H. Macek, Wave functions for continuum states of charged fragments, Phys. Rev. A **49**, 1049 (1994).

[40] E. Wang, X. Ren, M. Gong, E. Ali, Z. Wang, C. Ma, D. Madison, X. Chen, and A. Dorn, Triple-differential cross sections for (e, 2e) electron-impact ionization dynamics of tetrahydrofuran at low projectile energy, Phys. Rev. A **102**, 062813 (2020).

[41] A. G. Sanz, M. C. Fuss, A. Muñoz, F. Blanco, P. Limão-Vieira, M. J. Brunger, S. J. Buckman, and G. García, Modelling low energy electron and positron tracks for biomedical applications, Int. J. Radiat. Biol. **88**, 71 (2012).

[42] M. U. Bug, W. Yong Baek, H. Rabus, C. Villagrasa, S. Meylan, and A. B. Rosenfeld, An electron-impact cross section data set (10 eV–1 keV) of DNA constituents based on consistent experimental data: A requisite for Monte Carlo simulations, Radiat. Phys. Chem. **130**, 459 (2017).